

Self-Assembly of Polymer-Coated Ferromagnetic Nanoparticles into Mesoscopic Polymer Chains

JASON J. BENKOSKI,¹ STEVEN E. BOWLES,² RONALD L. JONES,¹ JACK F. DOUGLAS,¹ JEFFREY PYUN,² ALAMGIR KARIM¹

¹Polymers Division, National Institute of Standards and Technology, Gaithersburg, Maryland 20899

²Department of Chemistry, University of Arizona, Tucson, Arizona 85721

Received 9 July 2007; revised 5 August 2008; accepted 7 August 2008

DOI: 10.1002/polb.21558

Published online in Wiley InterScience (www.interscience.wiley.com).

ABSTRACT: The self-assembly of dispersed polymer-coated ferromagnetic nanoparticles into micron-sized one-dimensional mesostructures at a liquid–liquid interface was reported. When polystyrene-coated Co nanoparticles (19 nm) are driven to an oil/water interface under zero-field conditions, long ($\approx 5 \mu\text{m}$) chain-like assemblies spontaneously form because of dipolar associations between the ferromagnetic nanoparticles. Direct imaging of the magnetic assembly process was achieved using a recently developed platform consisting of a biphasic oil/water system in which the oil phase was flash-cured within 1 s upon ultraviolet light exposure. The nanoparticle assemblies embedded in the crosslinked phase were then imaged using atomic force microscopy. The effects of time, temperature, and colloid concentration on the self-assembly process of dipolar nanoparticles were then investigated. Variation of either assembly time t or temperature T was found to be an interchangeable effect in the 1D organization process. Because of the dependence of chain length on the assembly conditions, we observed striking similarities between 1D nanoparticle self-assembly and polymerization of small molecule monomers. This is the first in-depth study of the parameters affecting the self-assembly of dispersed, dipolar nanoparticles into extended mesostructures in the absence of a magnetic field. ©2008 Wiley Periodicals, Inc. *J Polym Sci Part B: Polym Phys* 46: 2267–2277, 2008

Keywords: colloids; conformational analysis; imaging; nanoparticles; self-assembly; self-organization

Certain commercial equipments, instruments, or materials are identified in this article in order to specify the experimental procedure adequately. Such identification is neither intended to imply recommendation or endorsement by the National Institute of Standards and Technology, nor intended to imply that the materials or equipment identified are necessarily the best available for the purpose.

Correspondence to: J. J. Benkoski or J. Pyun (E-mail: jason.benkoski@jhuapl.edu or jpyun@email.arizona.edu)

Journal of Polymer Science: Part B: Polymer Physics, Vol. 46, 2267–2277 (2008)
© 2008 Wiley Periodicals, Inc. *This article is a US Government work and, as such, is in the public domain in the United States of America.

INTRODUCTION

The concept of using nanoparticles as colloidal “atoms” or “molecules” has gained significant attention as a bottom-up methodology to prepare ordered mesostructured materials. Examples of this approach include the cocrystallization of binary mixtures of monodisperse nanoparticles,¹ chemical linking of divalent nanoparticles,² and controlled assembly of latex colloids.³ The use of magnetic associations to organize nano- and meso-structured materials is of particular interest, as the directionality embedded from magnetic

dipoles enables selective 1D assembly of magnetic nanoparticles. While the 1D association of magnetic particles has long been known in the fields of ferrofluids⁴ and magnetorheological fluids,⁵ these systems primarily focused on field-induced changes in the volume, or viscosity of the magnetic fluid. The advantages of using nanoscale magnetic colloids as building blocks for self-assembly have been demonstrated in the formation of complex labyrinth structures,^{6–8} 2D crystals,^{9,10} and 3D superlattices,^{11–14} which have been formed in this fashion, resulting in materials with novel properties. Furthermore, magnetic field-induced 1D assembly of functional latex particles, or emulsion droplets impregnated with superparamagnetic iron oxide colloids has been achieved to form assembled chains spanning several microns in length. These structures have been used to prepare mesoscopic brush-like films, templates for inorganic metal oxides, and mechanical sensors.^{15–17}

Although these examples demonstrate the ability to use magnetic assembly to form novel materials, the use of ferromagnetic nanoparticles as “colloidal molecules” capable of 1D organization remains a difficult challenge. One of the fundamental problems using this approach is the preparation of uniform, ferromagnetic colloids that are capable of retaining a dipole moment and inducing dipolar associations at room temperature. Numerous methods have been reported for the preparation of superparamagnetic nanoparticles using either small molecule or polymeric surfactants. However, the synthesis of well-defined ferromagnetic colloids are significantly more demanding because of the requirement of growing particles to larger sizes, while suppressing flocculation of nanoparticle from dipolar associations. Ferromagnetic colloids of metallic cobalt nanoparticles have been previously synthesized with small molecule surfactants.^{18,19} We have recently improved upon the preparation of these materials, by the use of end-functionalized polymers that enable the preparation of uniform ferromagnetic nanoparticles with enhanced colloidal stability.²⁰

An intriguing analogy exists between self-assembled nanoparticle chains and traditional polymer molecules on meso- and nanoscopic regimes. Magnetically self-assembled 1D mesostructures are reminiscent of nanoscale polymeric macromolecules, which we refer to as mesoscopic polymer chains, or, simply, “mesopolymers.” Nanoparticle self-assembly offers many possibilities to prepare mesopolymer structures by bor-

rowing concepts from polymer chemistry, namely, control of chain length, architecture, length polydispersity, and sequence.

Characterization of magnetic nanoparticle assembly has been widely investigated both computationally^{21–23} and experimentally on surfaces as thin films.^{6–14,24–26} A fundamental problem encountered with the assembly and imaging of very small dispersed magnetic nanoparticles is the facile perturbation of the dipolar associations from thermal fluctuations (i.e., Brownian motion). This effect can be overcome to some degree by the application of strong magnetic fields, but it is an inherent limitation when dealing with nanoparticles. Monte Carlo simulations have shown that dispersed ferromagnetic nanoparticles will assemble under certain conditions into chains and rings in the absence of a magnetic field.^{21,22} However, experimental demonstrations of magnetic assembly of dipolar colloids has been inhibited by synthetic limitations and a lack of versatile measurement methodologies.

The visualization of nanoparticle assembly in solution is a critical aspect of understanding the formation of mesopolymer structures. In particular, the assessment of defects in nanoparticle assemblies is important in determining structure–property correlations for self-assembled materials prepared using “bottom-up” approaches. Although dilute solution scattering techniques can provide detailed information about the structure of a ferrofluid,^{27–29} differentiation of discrete polymer topologies such as random branching, comb-like branching, or star morphologies is difficult to verify without independent measurements. The precise morphology of individual assemblies and defect sites is perhaps best determined by direct imaging.

Recent work by Philipse and coworkers^{30–32} has experimentally confirmed the magnetic assembly of dipolar colloids using cryogenic transmission electron microscopy (cryo-TEM) to visualize frozen assemblies of ferrimagnetic magnetite (Fe₃O₄) nanoparticles (particle size = 18 nm). These promising findings suggest that the dipolar association of functional magnetic nanoparticles is a viable route to form 1D mesoscopic structures. Although cryo-TEM is a powerful tool probe colloidal dispersions, investigation in certain organic media is often complicated. To address this issue, we have recently developed a versatile measurement platform, named fossilized liquid assembly (FLA), that utilizes an oil/water interface.^{33,34} With this system, nanoparticles in either phase

are driven to the interface, where the oil phase is then solidified in less than 1 s using ultraviolet (UV) light exposure. Nanoparticles are allowed to organize at the interface and curing of the oil phase preserves a “snapshot” of the assembly process at the instant of UV exposure. One can then image the resulting assemblies *ex situ* atop the cured polymer film using atomic force microscopy (AFM). The FLA methodology allows direct monitoring self-assembly processes, particularly, of imaging small, delicate, and highly mobile structures in a liquid medium. These conditions are especially problematic given that most microscopy techniques either suffer from slow scan rates or require measurements performed in vacuum. Existing adaptations generally involve tedious sample preparation steps, many of which can perturb the morphology of assembled structures and introduce artifacts. The key challenge, then, is to provide a facile, noninvasive measurement methodology for imaging nanoparticle assembly under a wide variety of assembly conditions (e.g., particle concentration, temperature, applied field).

In this study, we report the magnetic self-assembly of dispersed ferromagnetic polystyrene-coated cobalt nanoparticles (PS-CoNPs) into micron-sized mesoscopic polymer chains at the interface between water and 1,12-dodecanediol dimethacrylate (DDMA). Using the FLA methodology, the effect of varying conditions on the magnetic assembly was investigated and self-assembly to form mesoscopic polymer chains was visualized. Equilibrium polymerization theory was utilized as a theoretical framework for understanding the effects of particle concentration, time, and temperature. Using quantitative image analysis (QIA), we determined the morphology and dimension of mesopolymers, which enabled optimization of conditions for the assembly of magnetic colloids. This is the first demonstration of 1D self-assembly and direct visualization of dispersed ferromagnetic nanoparticles into micron-sized mesopolymer chains, in particular, as a function of time, temperature, and concentration.

EXPERIMENTAL

Materials and Instrumentation

Irgacure 819 (bis(2,4,6-trimethylbenzoyl)phenylphosphine oxide) was purchased from Ciba Specialty Chemicals and used as received. DDMA and *N*-(2-hydroxyethyl)piperazine-*N'*-2-ethanesulfonic acid (HEPES) were purchased from Aldrich

and used as received. Tapping mode AFM was conducted using an Asylum Research MFP-3D AFM scope. TEM images were obtained on a JEM100CX II transition electron microscope (JEOL) at an operating voltage of 60 kV, using in-house prepared copper grids (Cu, hexagon, 270 mesh).

Synthesis of Polystyrene-Coated Ferromagnetic Colloids

Polystyrene (PS) surfactants and ferromagnetic cobalt nanoparticles were prepared using our previously reported methodology.²⁰

Sample Preparation

³⁴PS-Co colloids were first dispersed in bulk DDMA by sonication for 30 min. Figure 2 illustrates the experimental setup for performing 2D particle aggregation. It consists of an oil phase, a water phase, and a solid glass support for the oil phase. To promote wetting and adhesion with the oil phase, the glass slide was pretreated with silane and crosslinked DDMA.

The oil phase consisted of DDMA modified with 2% Irgacure 819 by mass fraction (all percentages refer to mass fraction throughout this article) to promote rapid crosslinking during UV light exposure. With a viscosity of 15 mPa s, DDMA has similar flow properties to water at room temperature (0.89 mPa s). The aqueous phase was buffered using 10 mM HEPES. The pH was adjusted to 8, and the salt concentration was fixed at 100 mM NaCl to help prevent emulsification of water in the oil phase. The interfacial tension between these two fluids is $\sim 15 \text{ mJ/m}^2$ at 25 °C, which is a similar magnitude as that between water and cooking oil. The high interfacial tension facilitates the partitioning of the nanoparticles to the interface, which do so with a well-defined equilibrium constant that varies with the thermodynamic conditions. Depending upon the concentration of nanoparticles in the bulk DDMA phase, the equilibrium constant determines the areal density of particles at the interface at any given instant. Therefore, even though the PS shell on the Co nanoparticles is relatively hydrophobic, the Co nanoparticles will still populate the interface so long as the bulk concentration is sufficiently high. Of course, the implication of weak interfacial segregation is that self-assembly occurs within the bulk DDMA phase as well. We believe that the two-dimensional confinement

imposed by the high interfacial tension may affect the morphology of the self-assembled structures somewhat, and so we restrict our observations to the planar structures on the DDMA surface.

Complete solidification of the DDMA phase, or “fossilization,” takes place in less than 1 s when the sample is exposed to a 365 nm high pressure mercury lamp at an intensity of 8 mW/cm². Although 1 s is a relatively short time to achieve a full cure, a nanoparticle actually diffuses over a relatively large distance during this time. The question, then, is whether diffusion during the cure time can lead to distortion of the final aggregate. Unless curing results in local hot spots, lateral heterogeneities during gel formation, convective currents, or a Marangoni effect, a gradual increase in viscosity should impose no bias on the diffusion paths that lead to the final structure. Rather, a smooth increase in viscosity from 15 mPa s to infinity should merely result in a slowing of kinetics during the cure time. As for the other possibilities, the small thickness of the oil layer (ca. 100 μm) and the high thermal conductivity and heat capacity of water help to mitigate thermal sources of flow-induced anisotropy. The high concentration of photoinitiator and high intensity of the UV light also help to mitigate chemical sources of heterogeneity. For systems such as this, photocuring generally proceeds as a frontal polymerization in which the conversion profile propagates downwards from the illuminated surface as a traveling wave of network solidification through the unpolymerized medium.

Sample preparation was varied with respect to particle loading (0.01, 0.02, 0.07, 0.11, and 0.20%), *T* (22, 50 °C), and assembly time before UV curing time *t* (1, 5, 15, 30, 60 min).

Image Analysis

For each image, QIA was performed to obtain average values for the contour length of the chains (*L*), the polydispersity index (PDI), the radius of gyration (*R_g*), the fractal dimension (*d_f*), the areal density of all chain-like aggregates (*ρ_{chain}*), the areal density of branches (*ρ_{branch}*), and the areal density of rings (*ρ_{rings}*). Ten-micrometer-scale scans were used from each sample because this was the lowest magnification for which individual nanoparticle assemblies could be well resolved. The first step of the analysis was to manually trace lines over each nanoparticle chain. The lines were then converted into a binary image, which was then analyzed by Igor Pro[®] 5.0 to obtain the

length in pixels (*L*), Σx , Σy , Σx^2 , and Σy^2 for each chain, where *x* and *y* refer to the coordinates of the pixels along the *x* and *y* axes, respectively. *R_g* can then be calculated according to the following equation:

$$R_g = \left[\frac{1}{L} \Sigma x^2 - \left(\frac{1}{L} \Sigma x \right)^2 + \frac{1}{L} \Sigma y^2 - \left(\frac{1}{L} \Sigma y \right)^2 \right]^{1/2} \quad (1)$$

The pixel values are then converted to units of μm by using the appropriate calibration factor for each image. With *R_g* calculated, one can obtain the fractal dimension (*d_f*) by making a log–log plot of *L* versus *R_g* and taking the slope.

The PDI was calculated as usual according to the ratio of the weight average and number average molecular weight. However, in this case the molecular weight was substituted with *L*:

$$\text{PDI} = \frac{\sum_{i=1}^n n_i L_i^2}{\sum_{i=1}^n n_i L_i} \left(\frac{\sum_{i=1}^n n_i L_i}{\sum_{i=1}^n n_i} \right)^{-1} \quad (2)$$

where *n_i* is the number of chains of length, *L_i*.

RESULTS AND DISCUSSION

Synthesis of PS-CoNPs

We have recently developed a robust synthetic process to prepare polymer-coated cobalt nanoparticles that exhibit ferromagnetism at room temperature and to form stable colloidal dispersion in various organic solvents.²⁰ These organic/inorganic hybrid nanomaterials were prepared using a hierarchical synthetic methodology, in which end-functionalized PS containing amine, or phosphine oxide end-groups was prepared using controlled radical polymerization. These end-functionalized chains were then used in the thermolysis of dicobaltoctacarbonyl (Co₂(CO)₈) to prepare ferromagnetic cobalt nanoparticles. The low-molar-mass PS surfactants (*M_n* = 5000 g/mol; *M_w*/*M_n* = 1.10) passivate the colloidal surface by ligation of chain ends to stabilize the nanoparticle. The presence of the polymer shell enables dispersion of the ferromagnetic colloids in non-polar organic media (e.g., toluene, tetrahydrofuran, dichloromethane). Solid-state and magnetic characterization of these polymer-coated colloids

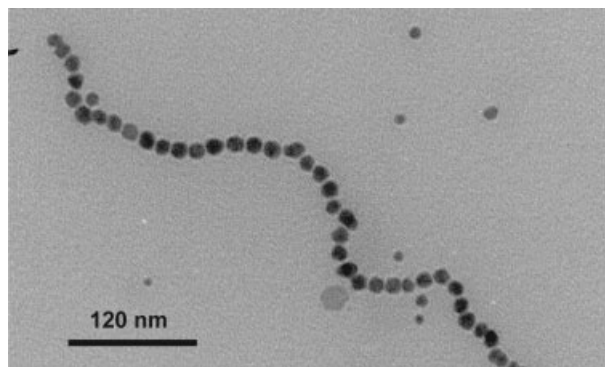


Figure 1. TEM of ferromagnetic PS-coated cobalt nanoparticles ($D = 19$ nm) deposited onto carbon-coated copper grids from toluene dispersions (0.1 mg/mL).

confirmed the presence of f.c.c. metallic cobalt that exhibited weak ferromagnetism at room temperature ($M_s = 38$ emu/g, $H_c = 100$ Oe, $T = 22$ °C). When cast onto surfaces, these polymer-coated colloids organize into micron-sized chains, as evidenced by TEM, because of dipolar associations. Particle sizes from TEM displayed good uniformity ($D = 19 \pm 1.5$ nm, $D_{\text{Co core}} = 15$ nm, PS shell = 2 nm), ensuring that the particles would serve as excellent model systems to probe assembly processes in the dispersed state (Fig. 1).

To evaluate the ability of dispersed ferromagnetic PS-CoNPs to self-assemble into mesopolymer chains under zero-field conditions, FLA was utilized to systematically investigate the effects of particle concentration, assembly time and temperature (Fig. 2).

Effects of Particle Concentration

The AFM micrographs in Figure 3 depict PS-Co nanoparticles at the crosslinked DDMA surface (PDDMA) after a 5-min assembly time at constant temperature ($T = 22$ °C). At the lowest concentration (0.01%), aggregation was not observed; however, at 0.02%, string-like self-assembly of colloids into linear mesopolymer chains occurred. The organized chains themselves were one nanoparticle wide and up to several μm in length. In these mesopolymer assemblies, the conformation strongly resembled the self-avoiding random walk of a polymer chain.

The contour length and areal density of the mesopolymers tend to increase with increasing mass fraction from 0.02 to 0.11%, but at 0.20% fewer chains are present because of the competing formation of globular clusters. In fact, the chain-like aggregates at 0.20% were often several particles thick and appeared to be showing early signs of transformation into globular aggregates.

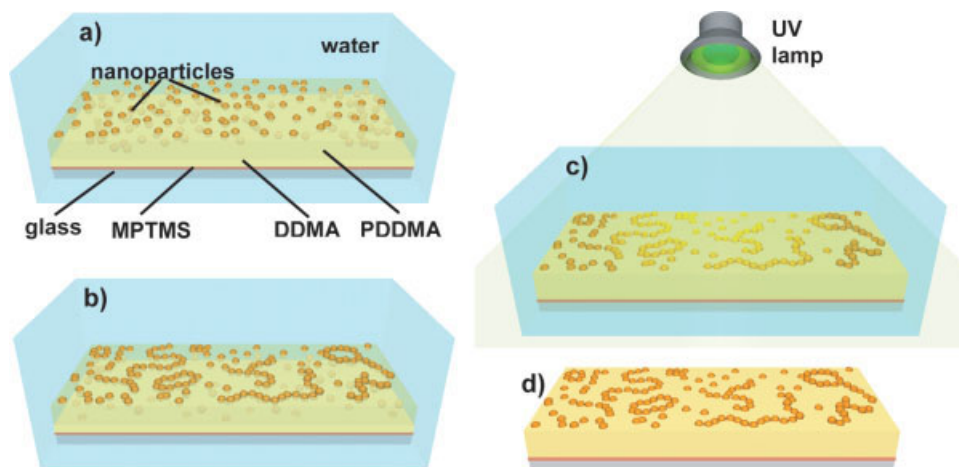


Figure 2. Schematic of self-assembly samples showing DDMA-coated glass slides immersed in water. (a) The PS-Co nanoparticles are initially dispersed in the DDMA, sonicated, and then placed on a glass slide that is precoated with a layer of adhesion promoter (MPTMS) and a layer of crosslinked DDMA (PDDMA). (b) Once the slide is immersed in water, the particles are given time to segregate to the interface and self-assemble. (c) The assembly is then “fossilized” by crosslinking the DDMA with UV light. (d) Finally, the solidified sample is removed from water, dried, and then inspected using atomic force microscopy. [Color figure can be viewed in the online issue, which is available at www.interscience.wiley.com.]

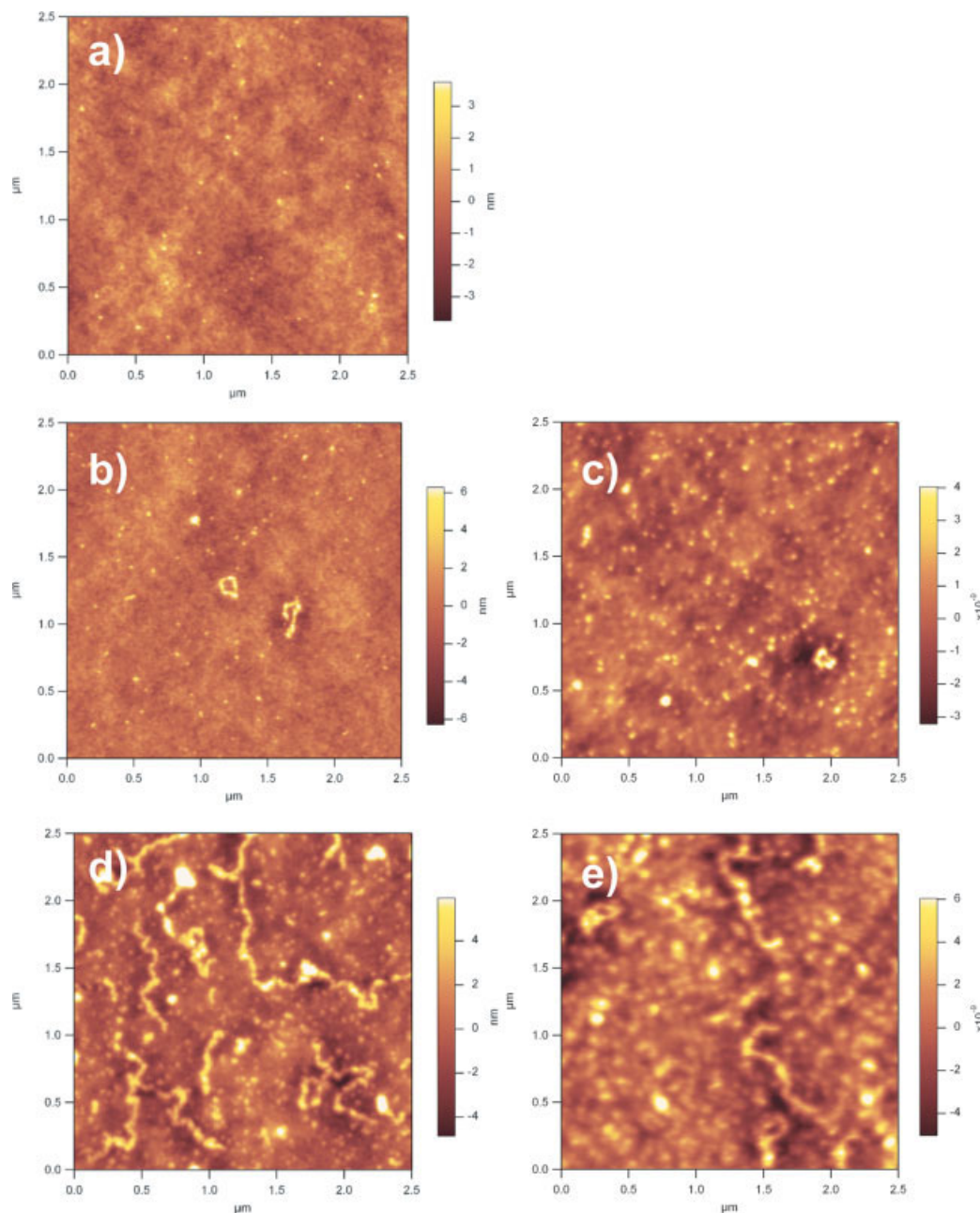


Figure 3. AFM height images of self-assembled PS-Co nanoparticles as a function of concentration. Each sample was prepared at 22 °C for 5 min. The concentration was varied as follows: (a) 0.01%, (b) 0.02%, (c) 0.07%, (d) 0.11%, and (e) 0.20% by mass fraction. Observe that chain-like aggregates were formed at all concentrations except 0.01%. At the highest concentration, 0.20%, nearly the entire surface is coated with particles. [Color figure can be viewed in the online issue, which is available at www.interscience.wiley.com.]

At lower concentrations, the chains formed either short chains or rings in approximately equal numbers. Branching was not evident until the concentration exceeded 0.11%, and it became more prevalent with increasing concentration.

Effects of Time

The assembly time for sample preparation was also investigated at a set particle concentration (0.07% by mass fraction) and temperature ($T = 22$ °C) for development periods of 1, 5, 15, 30, and

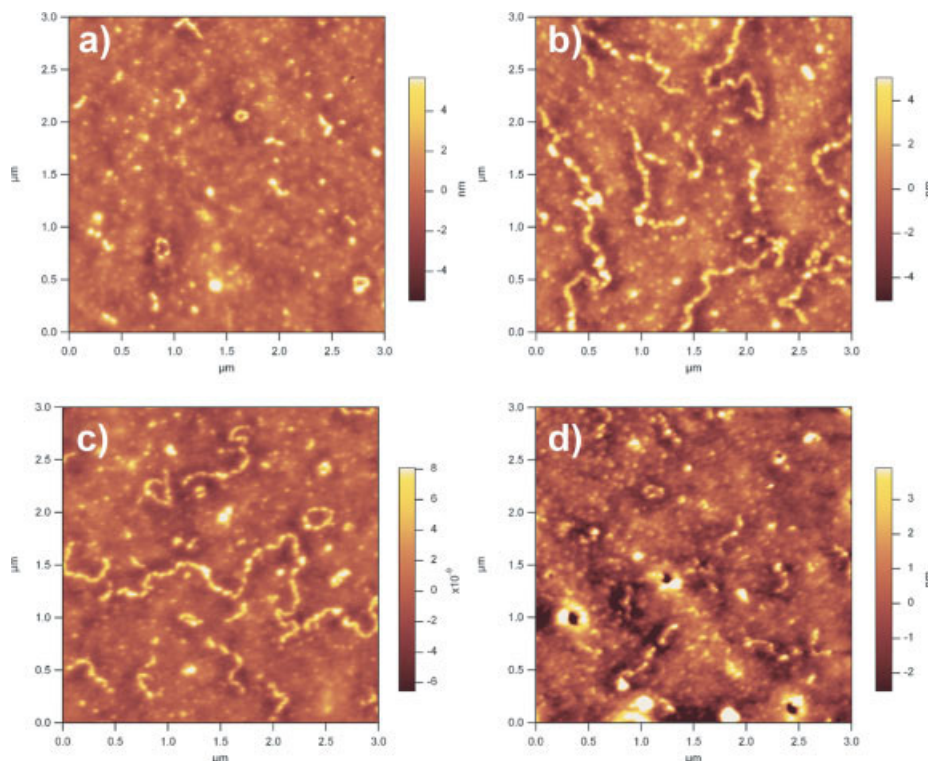


Figure 4. Evolution of nanoparticle chains as a function of time for a concentration of 0.07% Co nanoparticles by mass fraction. The AFM height images were obtained after allowing (a) 1, (b) 15, (c) 30, and (d) 60 min for self-assembly at $T = 22\text{ }^{\circ}\text{C}$. [Color figure can be viewed in the online issue, which is available at www.interscience.wiley.com.]

60 min. As shown in Figure 4, chain lengths of the seven assembled mesopolymers increased with longer development times. The appearance at 15 min was not significantly different from that at 30 min, indicating that the system may be approaching equilibrium or a steady state.

In general, the number of chains, aggregates, and free nanoparticles appeared to increase to a maximum value somewhere between 15 and 30 min. Shorter times afforded more well-defined assemblies consisting only of chains and free particles. The fact that macroscopic sedimentation occurred in the oil layer at long times suggests that globular cluster formation competes with chain formation, with cluster formation dominating at longer times.

Effects of Temperature

The temperature was increased to $50\text{ }^{\circ}\text{C}$ by placing the sample chamber in contact with a large water bath, and the experiments were repeated at 0.02, 0.07, 0.11, and 0.20% mass fractions (Fig. 5). For all samples below a 0.20% particle loading,

the chain lengths of the mesopolymers increased with higher particle concentrations. However, at higher particle concentrations, mesopolymer formation was not observed, as Co colloids nearly formed a complete monolayer between the oil and water layers [Fig. 5(d)]. At this concentration, particle aggregates are difficult to discern from the background of free particles. Another set of samples (not shown) were developed at $50\text{ }^{\circ}\text{C}$ for 5 min followed by $22\text{ }^{\circ}\text{C}$ for 5 min. These experiments were performed to determine whether the effects of temperature were reversible or history dependent. Except for possibly a greater number of aggregates, the samples were nearly identical to the $50\text{ }^{\circ}\text{C}$ samples shown in Figure 5, indicating that the temperature effects were, in fact, history dependent. The formation of mesopolymer chains from PS-CoNPs is evident in 3D AFM height images, which indicates that these organize into 1D mesostructures, flux-closure rings, and branched polymer assemblies [Fig. 6(a,b)].

A comparison of samples prepared under identical particle loadings (0.07%) but under different

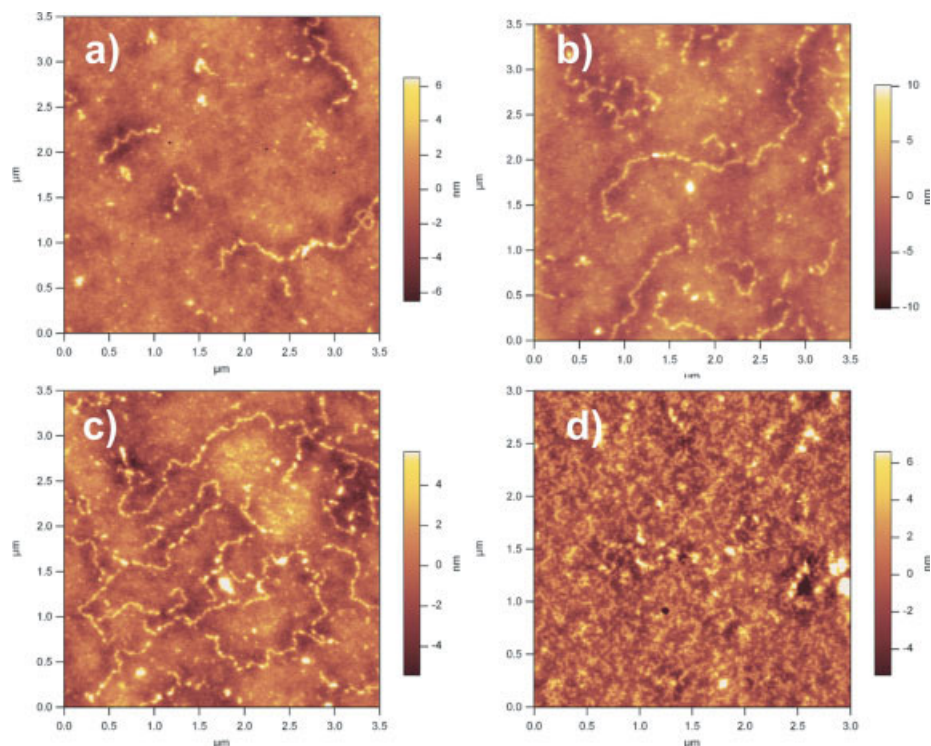


Figure 5. AFM height images of PS-Co nanoparticles self-assembled at 50 °C for 5 min. The concentrations are as follows: (a) 0.01%, (b) 0.07%, (c) 0.11%, and (d) 0.20% by mass fraction. In comparison with the structures formed at 22 °C, the chains are much longer, except in the case of (d), where the particle coverage was so dense that individual chains could not be identified. [Color figure can be viewed in the online issue, which is available at www.interscience.wiley.com.]

assembly conditions was carried out. Figure 5(b) shows a sample prepared for a time of 5 min at 50 °C, while Figure 4(b,c) shows samples prepared for 15 and 30 min at 22 °C. These images reveal the formation of mesopolymer chains having a similar morphology and show that similar chain lengths are obtained after these relatively long assembly times. These similarities confirm the expected correlation of increasing assembly time and temperature with longer chain lengths of organized mesopolymer chains.

Polymer Statistics

Although scattering methods are more efficient than AFM for obtaining chain morphology statistics, QIA of crosslinked phases provides both mole-fraction weighted values of chain lengths and distributions. The standard deviation, which serves as the standard statement of uncertainty, was generally high, as all averages only involved between 20 and 150 chains. Figure 7 summarizes

the image analysis data, and confirms the observations discussed in the previous sections. Namely, ρ_{chain} and L increase with increasing concentration. For a fixed time and concentration, ρ_{chain} and L increase with increasing temperature. The dependence of these chain properties on time at a fixed bulk particle concentration is more complicated; both ρ_{chain} and the apparent value of L reach a maximum between 15 and 30 min. Examination of the AFM images of the structures formed at such late times indicates that these decreases in ρ_{chain} and L arise from the nanoparticle chains collapsing into the globular structures, following the chain-assembly process during which ρ_{chain} and L grow. This phenomenon is strikingly reminiscent of the assembly behavior observed in the Stockmayer fluid³⁵ under conditions where there is a strong dipolar interaction in competition with a strong, attractive van der Waals interaction leading to phase separation and particle chain collapse. Simulations have shown a similar general tendency for self-assembly to form

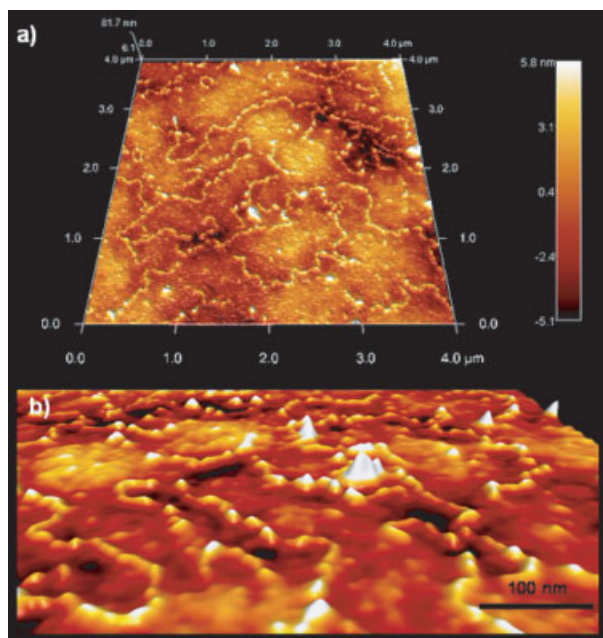


Figure 6. (a) 3D AFM height image of PS-CoNP mesopolymer chains self-assembled at 50 °C for 5 min [0.11% mass fraction of colloids shown in Fig. 5(c)]; (b) high-magnification 3D AFM of PS-CoNP mesopolymer chains from Figure 5(c).

chains to precede collapse, presumably because the repulsive dipolar interactions are largely negated in the assembled chain clusters which then become sensitive to residual van der Waals interactions.³⁶ These collapsed nanoparticle chain droplets fall out of the interface because of sedimentation, resulting in a decrease of ρ_{chain} and the apparent value of L . Evidently, it will be necessary to modify the chain functionalization of the nanoparticles to weaken the van der Waals interactions enough to avoid this late-stage chain collapse phenomenon.

The PDI of the dipolar chains was relatively constant within the scatter of the data and it fluctuated around an average value of 1.5 with a standard deviation of 0.2. The relatively large PDI was reflected in the standard deviations of the individual L values, which tended to exceed 50% under all conditions. Also showing weak dependence on polymerization conditions was d_f . The average value was 1.19 with a standard deviation of only 0.01, slightly less than the value of 4/3 expected for a self-avoiding random walk in two dimensions. In Monte Carlo simulations, Van Workum and Douglas³⁶ also found that d_f for chains of spherical dipolar particles formed under equilibrium conditions

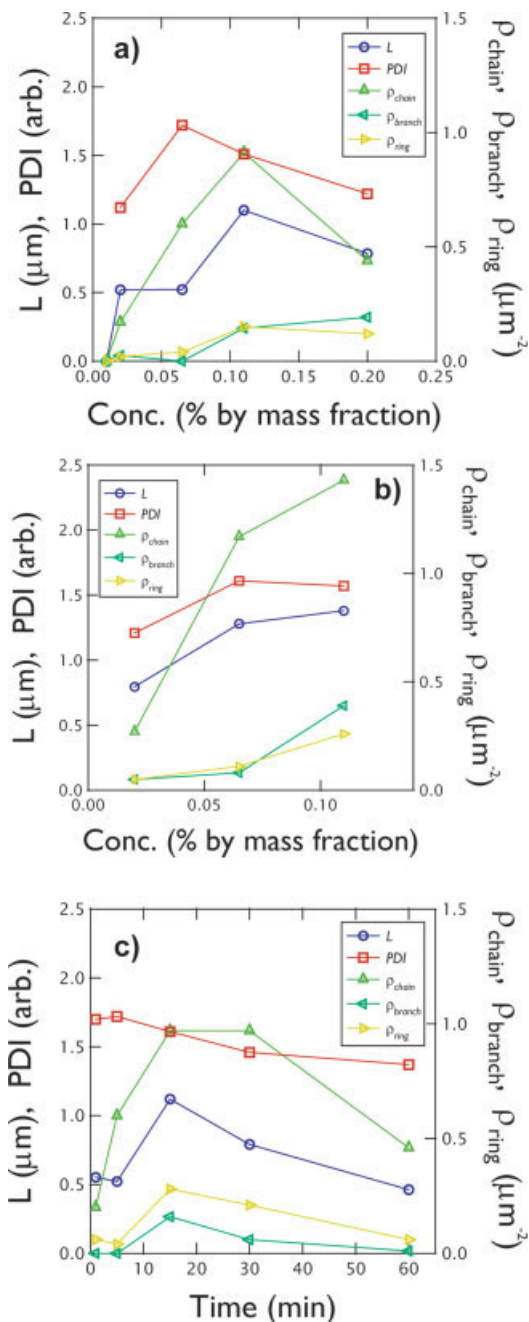


Figure 7. Image analysis data for the contour length, polydispersity index, areal chain density, areal branch density, and areal ring density for nanoparticle chains formed under zero-field conditions. The plot in (a) displays the data for samples prepared at 22 °C for 5 min, the plot in (b) displays the data for samples prepared at 50 °C for 5 min, and the plot in (c) displays the data for samples with a constant concentration of 0.07% by mass fraction as a function of time at 22 °C. Blue circles represent the L , red squares represent the polydispersity index (PDI), dark green triangles represent ρ_{chain} , aqua triangles represent ρ_{branch} , and light green triangles represent ρ_{ring} .

was roughly consistent with polymer chains having excluded volume interactions, perhaps with some degree of chain stiffness arising from the dipolar interactions. In particular, they found that the apparent d_f value in their simulations to be somewhat smaller than the ideal self-avoiding random walk polymers in 3D.

The values for ρ_{branch} and ρ_{ring} correlated very strongly with each other. In particular, $(\rho_{\text{branch}} + \rho_{\text{ring}})/\rho_{\text{chain}}$ increased with increasing concentration [Fig. 7(a,b)]. The proportion of branched and ring polymer structures did not appear to change significantly as a function of temperature or time, however [Fig. 7(c)].

CONCLUSIONS

We have demonstrated that mesopolymer chains can be self-assembled using polymer-coated ferromagnetic Co nanoparticles in the absence of an external field. The assembled chains can grow in length up to 5 μm in length, and exhibit a scaling of the radius of gyration with particle (“monomer”) number that is similar to self-avoiding random walks in two dimensions. Indeed, these nanoparticle chains share many characteristics with organic polymers formed under equilibrium polymerization conditions:^{36,37} a well-defined average degree of polymerization, formation of branched chain architectures, ring formation, polydispersity, and random walk statistics. We found that an increase in concentration causes an increase in the number of chains per area, the contour length of the chains, and the probability of defects (Y-junctions). Initially, the number and length of the chains increases as the dipolar particles self-assemble into chains, a process dominated by the highly directional interactions of the dipolar particles. After the chains have grown to significant dimensions, however, attractive van der Waals interactions exert their influence and the particle chains then begin to collapse into globular structures much like synthetic organic polymers in a poor solvent. These collapsed or “globular” clusters subsequently fall out of the interface by sedimentation. Unfortunately, this late-stage chain collapse process makes it impossible for us to obtain truly equilibrium dipolar particle mesopolymers in the system which we are currently studying and it will evidently be necessary to tune the chemistry (e.g., by grafting density or chain length of the stabilizing chain layer on the nanoparticles) to diminish the attractive isotropic

interparticle interactions responsible for this collapse phenomenon. The reversible formation of dipolar chains of magnetic dipolar particles exhibiting the quantitative characteristics of equilibrium polymerization has recently been achieved in the case of thermalized macroscopic magnetic dipolar particles,³⁷ and we expect similar behavior for appropriately modified magnetic nanoparticles. In this study, the modest temperature range investigated results primarily in a change of the fluid viscosity and, thus, leads to a change of the relative nanoparticle mobility. An increase in temperature thus increases the rate at which the chain assembly and subsequent chain collapse occur. It should be possible to observe *reversible* assembly and disassembly of dipolar chains by varying thermodynamic parameters, such as temperature, over a large enough range to influence the thermodynamic stability of the particle system as in simulation studies.^{36,37} However, this will demand the adjustment of dipolar interactions so that the self-assembly transition occurs near the temperature range of the measurements (temperatures comparable to room temperature) and the adjustment of van der Waals interactions to avoid phase separation. This is a challenge for future synthesis efforts.

Fellowship support from National Research Council is gratefully acknowledged. Additional support for this project was provided by the Information Storage Industrial Consortium (INSIC), American Chemical Society-Petroleum Research Fund, and the University of Arizona. We also acknowledge Eric Amis from the Polymers Division at NIST for support of the project. In addition, we thank Joe Antonucci, Steve Hudson, Chris Stafford, and Mike Fasolka from the Polymers Division at NIST for measurements, for providing resources, and for their helpful discussions.

REFERENCES AND NOTES

1. Redl, F. X.; Cho, K.-S.; Murray, C. B.; O'Brien, S. *Nature* 2003, 423, 968–971.
2. DeVries, G. A.; Brunnbauer, M.; Hu, Y.; Jackson, A. M.; Long, B.; Neltner, B. T.; Uzon, O.; Wunsch, B. H.; Stellacci, F. *Science* 2007, 315, 358–361.
3. Manoharan, V. N.; Elsesser, M. T.; Pine, D. J. *Science* 2003, 301, 483–487.
4. Zahn, M. *J Nanoparticle Res* 2001, 3, 73–78.
5. Klingenberg, D. J. *AIChE J* 2001, 47, 246–249.
6. Germain, V.; Richardi, J.; Ingert, D.; Pileni, M. P. *J Phys Chem B* 2005, 109, 5541–5547.

7. Germain, V.; Pileni, M. P. *J Phys Chem B* 2005, 109, 5548–5553.
8. Germain, V.; Pileni, M. P. *Adv Mater* 2005, 17, 1424–1429.
9. Ramos, L.; Lubensky, T. C.; Dan, N.; Nelson, P.; Weitz, D. A. *Science* 1999, 286, 2325–2328.
10. Bao, Y.; Beerman, M.; Krishnan, K. M. *J Magn Magn Mater* 2003, 266, L245–L249.
11. Sun, S.; Murray, C. B.; Weller, D.; Folks, L.; Moser, A. *Science* 2000, 287, 1989–1992.
12. Murray, C. B.; Sun, S. H.; Gaschler, W.; Doyle, H.; Betley, T. A.; Kagan, C. R. *IBM J Res Dev* 2001, 45, 47–56.
13. Black, C. T.; Murray, C. B.; Sandstrom, R. L.; Sun, S. *Science* 2000, 290, 1131–1134.
14. Sun, S.; Murray, C. B. *J Appl Phys* 1999, 85, 4325–4330.
15. Furst, E. M.; Suzuki, C.; Fermigier, M.; Gast, A. P. *Langmuir* 1998, 14, 7334–7336.
16. Singh, H.; Laibinis, P. E.; Hatton, T. A. *Langmuir* 2005, 21, 11500–11509.
17. Singh, H.; Laibinis, P. E.; Hatton, T. A. *Nano Lett* 2005, 5, 2149–2154.
18. Hyeon, T. *Chem Commun* 2003, 927–934.
19. Pyun, J. *Polym Rev* 2007, 47, 231–263.
20. Korth, B. D.; Keng, P.; Shim, I.; Bowles, S.; Nebesny, K.; Tang, C.; Kowalewski, T.; Pyun, J. *J Am Chem Soc* 2006, 128, 6562–6563.
21. Chantrell, R. W.; Bradbury, A.; Popplewell, J.; Charles, S. W. *J Phys D: Appl Phys* 1980, 13, L119–L122.
22. Chantrell, R. W.; Bradbury, A.; Popplewell, J.; Charles, S. W. *J Appl Phys* 1982, 53, 2742–2744.
23. Morosov, K. I. *J Chem Phys* 2003, 119, 13024–13032.
24. Cheng, G.; Romero, D.; Fraser, G. T.; Hight Walker, A. R. *Langmuir* 2005, 21, 12055–12059.
25. Puntès, V. F.; Krishnan, K. M.; Alivisatos, A. P. *Science* 2001, 291, 2115–2117.
26. Tripp, S. L.; Pusztay, S. V.; Ribbe, A. E.; Wei, A. *J Am Chem Soc* 2002, 124, 7914–7915.
27. Hayter, J. B.; Pynn, R. *Phys Rev Lett* 1982, 49, 1103–1106.
28. Pynn, R.; Hayter, J. B.; Charles, S. W. *Phys Rev Lett* 1983, 51, 710–713.
29. Moeser, G. D.; Green, W. H.; Laibinis, P. E.; Linse, P.; Hatton, T. A. *Langmuir* 2004, 20, 5223–5234.
30. Butter, K.; Bomans, P. H. H.; Frederik, P. M.; Vroege, G. J.; Philipse, A. P. *Nat Mater* 2003, 2, 88–91.
31. Butter, K.; Philipse, A. P.; Vroege, G. J. *J Magn Magn Mater* 2002, 252, 1–3.
32. Klokkenburg, M.; Vonk, C.; Claesson, E. M.; Meeldijk, J. D.; Ern e, B. H.; Philipse, A. P. *J Am Chem Soc* 2004, 126, 16706–16707.
33. Benkoski, J. J.; Hu, H.; Karim, A. *Macromol Rapid Commun* 2006, 27, 1212–1216.
34. Benkoski, J. J.; Jones, R. L.; Douglas, J. F.; Karim, A. *Langmuir* 2007, 23, 3530–3537.
35. ten Wolde, P. R.; Oxtoby, D. W.; Frenkel, D. *Phys Rev Lett* 1998, 81, 3695–3698.
36. (a) Van Workum, K.; Douglas, J. F. *Phys Rev E* 2005, 71, 031502; (b) Van Workum, K.; Douglas, J. F. *Phys Rev E* 2006, 73, 031502.
37. Stambaugh, J.; van Workum, K.; Douglas, J. F.; Losert, W. *Phys Rev E* 2005, 72, 031301.